

Elevated tissue sodium concentration in malignant breast lesions detected with non-invasive ^{23}Na MRI

Ronald Ouwerkerk · Michael A. Jacobs · Katarzyna J. Macura · Antonio C. Wolff · Vered Stearns · Sarah D. Mezban · Nagi F. Khouri · David A. Bluemke · Paul A. Bottomley

Received: 14 August 2006 / Accepted: 7 December 2006 / Published online: 27 January 2007
© Springer Science+Business Media B.V. 2007

Abstract

Background The hypothesis that physiological and biochemical changes associated with proliferating malignant tumors may cause an increase in total tissue sodium concentration (TSC) was tested with non-invasive, quantitative sodium (^{23}Na) magnetic resonance imaging (MRI) in patients with benign and malignant breast tumors.

Methods ^{23}Na and ^1H MRI of the breast was performed on 22 women with suspicious breast lesions (≥ 1 cm) at 1.5 Tesla. A commercial proton (^1H) phased array breast coil and custom solenoidal ^{23}Na coil were used to acquire ^1H and ^{23}Na images during the same MRI examination. Quantitative 3-dimensional ^{23}Na projection imaging was implemented with negligible signal loss from MRI relaxation, or from radio-frequency field inhomogeneity, in less than 15 min. Co-registered ^1H and ^{23}Na images permitted quantification of TSC in normal and suspicious tissues on the basis of ^1H MRI contrast enhancement and anatomy, with histology confirmed by biopsy.

Results Sodium concentrations were consistently elevated in ($N = 19$) histologically proven malignant

breast lesions by an average of 63% compared to glandular tissue. The increase in sodium concentration in malignant tissue was highly significant compared to unaffected glandular tissue ($P < 0.0001$, paired t -test), adipose tissue, and TSC in three patients with benign lesions.

Conclusion Elevated TSC in breast lesions measured by non-invasive ^{23}Na MRI appears to be a cellular-level indicator associated with malignancy. This method may have potential to improve the specificity of breast MRI with only a modest increase in scan time per patient.

Keywords Breast cancer · Magnetic resonance imaging · ^{23}Na magnetic resonance · Sodium · Quantification

Introduction

The use of magnetic resonance imaging (MRI) in clinical breast cases is increasing due to the high sensitivity (~90–95%) and moderate specificity (~83%) of gadolinium contrast-enhanced (CE) MRI [1, 2]. The lower specificity of ^1H MRI leads to additional breast biopsies, frequently of benign breast tissue or focal lesions [3–5].

The specificity of an ^1H MRI breast exam could be improved by adding indices that provide more information about the physiology and metabolism of suspicious lesions [6]. One such measure is the choline level as measured by ^1H magnetic resonance spectroscopy (MRS) [7–9]. However, ^1H MRS, with volume elements (voxels) of >1 ml, does not yield high spatial resolution, and is often applied at single

R. Ouwerkerk (✉) · M. A. Jacobs · K. J. Macura · S. D. Mezban · N. F. Khouri · D. A. Bluemke · P. A. Bottomley

Division of MR Research, Russel H. Morgan Department of Radiology and Radiological Science, Johns Hopkins University, School of Medicine, 601 N. Caroline Street, JHOC 4241, Baltimore, MD 21287-0845, USA
e-mail: rouwerke@mri.jhu.edu

M. A. Jacobs · A. C. Wolff · V. Stearns
Sidney Kimmel Comprehensive Cancer Center, Johns Hopkins University, School of Medicine, Baltimore MD, USA

pre-determined locations, thereby introducing potential sampling errors.

Sodium (^{23}Na) MRI also yields useful information that reflects the physiological and biochemical state of diseased tissue. Sodium has been shown to be a very sensitive indicator of cellular integrity and cellular energy metabolism [10–13]. The tissue sodium concentration (TSC) in normal tissue is primarily determined by the ratio of the intracellular and extracellular volume fractions (IVF and EVF) and the sodium concentrations in those volume fractions. To the extent that electrolytes in the blood pool remain regulated, the extracellular concentration remains constant provided there is exchange with the blood pool. Therefore, increased TSC can arise from increases in interstitial space due to changes in cellular organization or increased vascular volume, or from increases in the intracellular sodium concentration due to impaired energy metabolism or other metabolic changes that affect sodium exchange across the cell membrane [14]. Note that while EVF is also a factor affecting Gd uptake and efflux in ^1H CE-MRI. Factors that determine Gd contrast agent uptake are vascular volume and interstitial volume (both comprising EVF) and the permeability of the barrier between the vascular and interstitial compartment [15]. The intracellular component of TSC is independent of those physiological factors and reflects impaired energy metabolism, and changes in trans-membrane ion transport that have been linked to increased cell proliferation [16] and invasion [17].

Indeed, tumor cell proliferation is accompanied by a change in intracellular pH as part of the signaling mechanism that initiates cell division [18]. Altered Na^+/H^+ exchange kinetics and an acidic extracellular microenvironment of the tumor cells both may result in increases in intracellular Na^+ concentration [19]. Increased intracellular sodium concentration [19–21], increased Na^+/H^+ transporter activity [22], and Na^+ -potassium (K^+) adenosine triphosphatase (Na^+/K^+ -ATPase) activity [23] have all been linked to tumor malignancy. Neutron activation analysis (NAA) reveals a 60% increase in sodium concentration measured in $\mu\text{g}/\text{g}$ dry weight in infiltrating ductal carcinomas compared to normal breast tissue [24]. Increased thallium (^{201}Tl) radionuclide uptake, reported in breast cancer, also provides indirect evidence of altered Na^+ and K^+ homeostasis. As a potassium analog, ^{201}Tl uptake into the cells is linked to Na^+/K^+ exchange through the energy-dependent Na^+/K^+ -ATPase. The uptake through this transporter is enhanced when the intracellular Na^+ concentration is high.

TSC measured by ^{23}Na MRI is shown to be elevated by about 50% in malignant brain tumors in humans

[11]. Preliminary conference reports suggest that ^{23}Na MRI can yield a full 3D image of the breast with smaller voxel sizes of ~ 0.2 ml in 10–15-min scans [7, 25]. The lesion location in ^{23}Na images can be accurately determined by co-registering high-resolution ^1H images acquired during the same MRI exam. Other preliminary results suggest a link between the level of elevation of TSC and morphologic changes associated with tumor regression observed in several breast cancer patients undergoing chemotherapy [26]. We therefore hypothesized that increases in EVF and intracellular sodium concentrations would lead to elevated TSC in malignant lesions, and now report the first non-invasive quantitative ^{23}Na MRI measurements of TSC in breast cancer to test whether such increases occur. We investigate whether measures of TSC differ among malignant tissue, normal glandular tissue, and benign lesions in patients with suspicious masses identified by CE ^1H MRI, and confirmed by biopsy.

Methods

Patients

Study subjects (female, $N = 22$ age 38–66; mean 52 ± 11 years) were recruited from patients presenting with suspicious findings on X-ray mammography (BI-RADS¹ 4, 5), ultrasound, or at clinical breast examination, and who were scheduled for biopsy with an estimated lesion size of 1 cm or more. The MRI examination was performed prior to biopsy in all cases. Our Institutional Review Board approved this protocol, and written, informed consent was obtained from all subjects prior to the MRI exam.

^1H MRI breast protocol

All MRI examinations were performed on a GE (General Electric Medical Systems, Waukesha, WI) 1.5 Tesla scanner, using a dedicated commercial bilateral phased array breast coil Medrad (Indianola, PA) for ^1H MRI, with the patient in the prone position. ^1H MRI was performed using sagittal, fat-suppressed, T_2 -weighted (T_2W), fast spin-echo (sequence repetition time, $\text{TR} = 5,700$ ms; echo time, $\text{TE} = 102$ ms), and T_1 -weighted (T_1W), fast spoiled gradient echo sequences (FSPGR; $\text{TR}/\text{TE} = 200/4.4$ ms; field-of-view, $\text{FOV} = 18\text{--}20 \times 18\text{--}20$ cm, adjusted to the size of the breast; matrix size, 256×192 ; slice thickness,

¹ ACR BI-RADS Breast Imaging Reporting and Data System, American College of Radiology.

4 mm with a 1 mm gap). In addition, fat-suppressed, 3-dimensional FSPGR T1W (TR/TE = 20/4 ms; matrix = 512 × 160; 2 mm slice thickness) imaging was performed before and after intravenous administration of 0.1 mmol/kg gadodiamide contrast agent (*Omni-scan*, General Electric Health Systems). The contrast agent was injected over 10 s, with MRI beginning immediately after completion of the injection. The contrast bolus was immediately followed by a 20 ml saline flush. Total scan time for the ^1H MRI protocol was less than 30 min.

Quantitative ^{23}Na MRI

For quantitative ^{23}Na MRI, a custom-made solenoid coil was used as an insert in a commercially available ^1H MRI bilateral phased array coil (Medrad, Indianola, PA). The 11 cm diameter, 8 cm long ^{23}Na solenoid coil yields a practically homogeneous B1 field over a large part of its volume and, despite some coupling with the ^1H coils, allows co-registered ^1H MRI images to be recorded with an adequate signal-to-noise ratio (SNR). A ring-shaped coil phantom filled with a 150 mM sodium solution served as a fiducial marker for image registration and as a reference for determining coil-loading factors.

A ^{23}Na twisted projection imaging sequence [27] was used with an adiabatic excitation pulse replacing the square pulse in the original sequence to eliminate the need for flip angle calibrations and corrections for B1 field inhomogeneity [28]. The high efficiency of the solenoid ^{23}Na breast coil allowed the adiabatic excitation pulse to be played out at approximately 3–5 times

the RF power level required for a same length 90° square pulse. This resulted in a homogeneous 90° excitation throughout the sample, with minimal T_2 relaxation losses during the pulse [28]. A TR of 100 ms, estimated to be 3–4 times the T1 of breast tissue, obviated the need for saturation corrections and the very short TE of 0.4 ms minimized T2 losses. Six averages from 1,240 projections were recorded in 12:24 min [27] for effective isotropic resolution of 6 mm (0.22 ml voxels). Set-up and acquisition of the ^{23}Na MRI scans took less than 15 min. The total MR exam time for this protocol was typically less than 45 min.

The ^{23}Na data were corrected for k -space sampling density, linearly gridded with a triangular kernel [29], and Fourier transformed to a 3-dimensional image of with a 22 cm FOV and 64 points in all dimensions.

The ^1H and ^{23}Na images were co-registered in Matlab (Mathworks, Natick, MA), using Matlab scripts developed in-house. With this software, intensity level contours can be copied between co-registered images to guide the placement of regions of interest (ROI) on the ^{23}Na images to determine TSC. An example of this contour level transfer between co-registered sagittal ^1H images and corresponding ^{23}Na images is shown in Fig. 1.

For the quantification of TSC in the breast, as a concentration reference, we used separate scans recorded of a polypropylene bag with 4l of a 40 mmol/l NaCl solution in water doped with 2 g/l CuSO_4 . We tested the method in the breast coil setting for SNR and linearity by imaging seven tubes filled with known concentrations of NaCl (30, 45, 60, 75 mmol/l) in aqueous agarose gel doped with CuSO_4 . The noise level

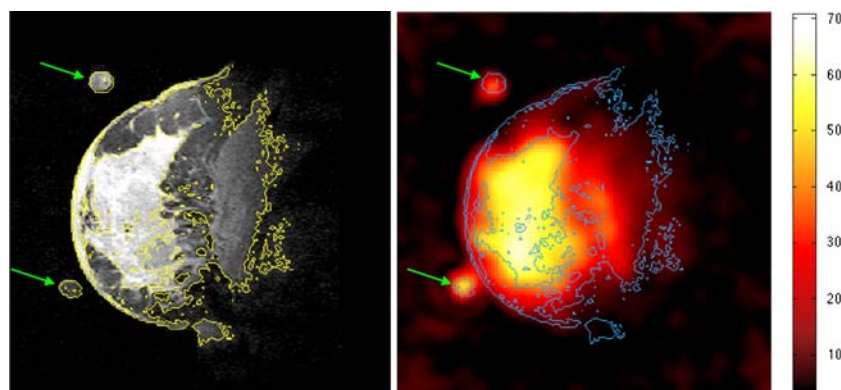


Fig. 1 Image registration of ^{23}Na and ^1H images. The images are from a 39-year-old patient (#10) with a very large locally advanced breast cancer, all of which show Gd uptake as well as high TSC. Level contours from the post-Gd injection T1W images (left, yellow contour lines) were copied to registered ^{23}Na images (right, blue contour lines). Green arrows indicate the position of the ring-shaped fiducial phantom. The color map for

the ^{23}Na images is shown on the right, with an image intensity scale that was adjusted to approximate the measured sodium concentrations (for actual TSC measurements, see the Materials and Methods section). Both the ^1H image and the ^{23}Na image were interpolated to a common resolution of 256×256 per image with 3.5 mm slice spacing

in each 3D ^{23}Na MRI data set was measured in a slice containing no features by averaging the absolute pixel intensity values over an ROI of 1–2 thousand pixels. All other intensity measures were corrected for noise by subtracting the mean noise value found in this ROI. The standard deviation of the noise in this ROI was used to calculate SNR for the breast tissues as:

$$\text{SNR}_{\text{tissue}} = \frac{\hat{I}_{\text{tissue}} - \hat{I}_{\text{noise}}}{\text{SD}_{\text{noise}}} \quad (1)$$

where \hat{I}_{tissue} and \hat{I}_{noise} are the mean absolute pixel intensity in the tissue and noise ROI, respectively, and SD_{noise} is the standard deviation of the noise in the noise ROI.

TSC was calculated from mean tissue intensities in the relevant ROI, \hat{I}_{tissue} , and the mean intensity found in that same location in a concentration reference scan of the 40 mmol/l concentration reference phantom, $\hat{I}_{\text{conc-ref}}$, according to Eq. (2). To correct the results for coil loading differences between patient scan (scan 1) and concentration reference scan (scan 2), we used the ratio of the (noise-corrected) signals of the ring-shaped phantom in the coil, \hat{I}_{ring} , measured from the scan with the patient and measured from the scan with the concentration reference phantom.

$$\text{TSC}_{\text{tissue}} = C_{\text{conc-ref}} \left[\frac{\hat{I}_{\text{tissue}} - \hat{I}_{\text{noise1}}}{\hat{I}_{\text{ring}} - \hat{I}_{\text{noise1}}} \right]_{\text{scan1}} \cdot \left[\frac{\hat{I}_{\text{ring}} - \hat{I}_{\text{noise2}}}{\hat{I}_{\text{conc-ref}} - \hat{I}_{\text{noise2}}} \right]_{\text{scan2}} \quad (2)$$

Statistical analysis

Statistical analyses were performed with Excel software (Microsoft, Redmond, CA) for all *t*-tests and Matlab for the Wilcoxon ranked tests. Sodium concentrations of different tissues within the patient group were tested with a paired two-tailed *t* test for the null hypothesis that the mean concentrations in the tissues were equal. Because the plasma sodium concentration is arguably the maximum achievable value of sodium concentration in lesions, it is conceivable that the concentration in lesions does not have a normal distribution around the means. To account for this, the sodium concentrations in malignant lesions and in remote unaffected glandular and adipose regions were also compared using a nonparametric Wilcoxon signed rank test.

For comparison of sodium concentrations in benign lesions with the TSC found in malignant lesions, an independent samples two-tailed *t*-test was used.

In all statistical comparison tests, the null hypothesis was that the sodium concentrations in the sample groups were equal with a significance cut-off level of .05. No Bonferroni corrections were applied because this correction is concerned with a general null hypothesis that all null hypotheses are true simultaneously [30], whereas in this study the focus is on the difference between TSC in healthy tissue and TSC in malignant lesions. Thus, *P* values of 0.05 or less were deemed indicative of a significant difference between the means.

Results

^{23}Na and ^1H MRI

Consistently good anatomical and fiducial marker correspondence was found between the ^1H and ^{23}Na images (Fig. 1). The excellent ^{23}Na MRI SNR and the linear relationship between the SNR and the sodium concentration is illustrated by the graph in Fig. 2. Even the tube with the lowest sodium concentration, 30 mmol/l NaCl, yielded an SNR of about 45. In human subjects, coil loading and increased sample noise

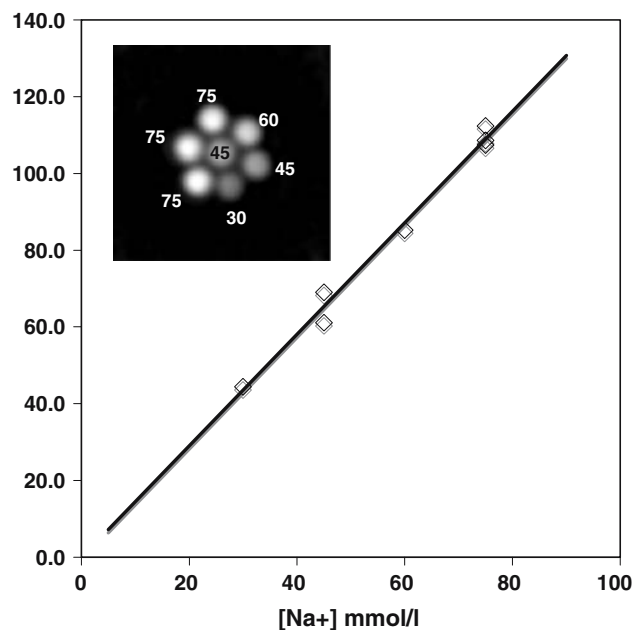


Fig. 2 SNR as a function of sodium concentration. Seven 2 cm-diameter tubes with known NaCl concentrations in aqueous agarose gels were measured with the ^{23}Na MR scan method used for patient studies. The mean pixel intensities in a 1.5 cm-diameter circular ROI centered on the tubes were used to calculate SNR. Insert: A coronal slice from the 3D data set with the labels indicating the concentration of NaCl in the phantom tubes

reduced SNR to 14 ± 8 ($N = 22$) in adipose tissue, to 32 ± 10 ($N = 19$) in non-involved glandular tissue, and to about 40 ± 17 ($N = 22$) in lesions.

Hyperintense areas in ^{23}Na images of patients correspond to hyperintense areas in the T1W images recorded after administration of contrast agent (Fig. 1), or to cysts or inflamed or edematous glandular tissue. Differentiation of edematous glandular tissue, cysts, and suspicious lesions is accomplished by the comparison of fat-suppressed T2W images, and the T1W images with contrast agent (Fig. 3). A complete set of registered ^1H and ^{23}Na images of a 63-year-old patient (#10) with infiltrating, poorly differentiated, ductal carcinoma with necrosis is shown in Fig. 4.

TSC in patients

Nineteen subjects had malignant tumors, and three subjects had benign lesions. The minimum lesion size of about 1 cm in the inclusion criteria may have contributed to the relatively low number of benign subjects. The biopsy results for the malignant lesions indicated invasive ductal carcinomas ($N = 14$), ductal carcinoma in situ (DCIS) ($N = 1$), and infiltrating lobular carcinomas ($N = 4$). The benign lesions were fibrocystic changes ($N = 1$, Fig. 5) and fibroadenomas ($N = 2$). Malignant lesions demonstrated an increased TSC of 53 ± 16 mmol/l ($N = 19$), compared to benign lesions (26 ± 5 mmol/l; $N = 3$), ($P < 0.0004$ with a two-tailed t -test assuming unequal variance). On average, TSC in malignant lesions was increased by more than 60% of the level in remote glandular tissue, whereas the TSC in benign lesions was about equal to that of the TSC found in non-involved, remote glandular tissue (34 ± 13 mmol/l; $N = 19$). In two-tailed, paired t -tests, the difference between TSC in malignant lesions

and non-involved glandular tissue was significant at $P < 5 \times 10^{-6}$ ($N = 19$) (Table 1).

In three of the 19 patients with malignant lesions, a reliable TSC reading in uninvolved glandular tissue was not possible. Patient #9 had three separate enhancing loci and uninvolved glandular tissue could only be found close to the nipple, coinciding with the boundaries of the reference phantom so that no concentration reference reading could be obtained for that region. However, the ratio of the signal intensity of the lesion to that in uninvolved glandular tissue was 2.3 ± 0.76 . Patient #10 had an extremely large lesion (Fig. 1) with insufficient unaffected glandular tissue available for a TSC reading. Patient #21 also had multiple large lesions and a high intensity sodium signal just under most of the skin, with little unaffected tissue available for TSC measurements. The region under the skin showed some Gd uptake, as well as the presence of some cysts visible in the T2W images. The TSC in one of the larger fluid pockets just under the skin was 60 mmol/l. A significant difference was also found for lesions versus adipose tissue ($N = 19$; $P < 0.0001$). The TSC measurements for all patients are shown in Fig. 6. Table 1 correlates the individual biopsy findings with the TSC results.

Discussion

Using non-invasive ^{23}Na MRI, we report for the first time that TSC is profoundly elevated in malignant breast lesions, as compared to normal glandular tissue. We demonstrate that ^{23}Na MRI can routinely deliver high SNR (~ 40) in human breast lesions at 1.5 Tesla, potentially permitting the detection of small changes in TSC and quantitative measurements of sodium levels

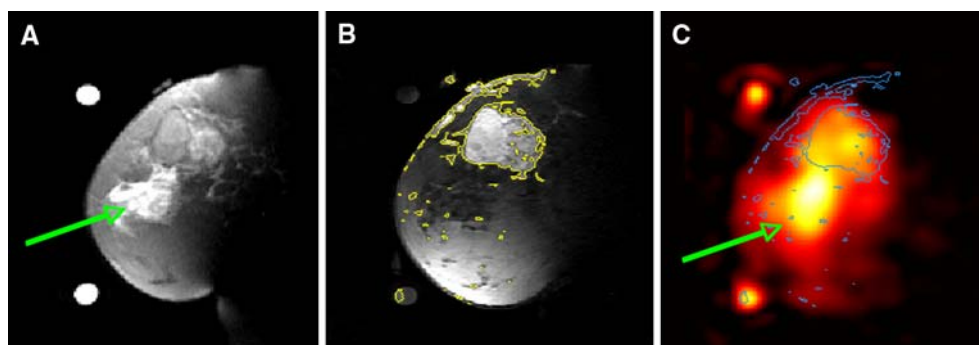
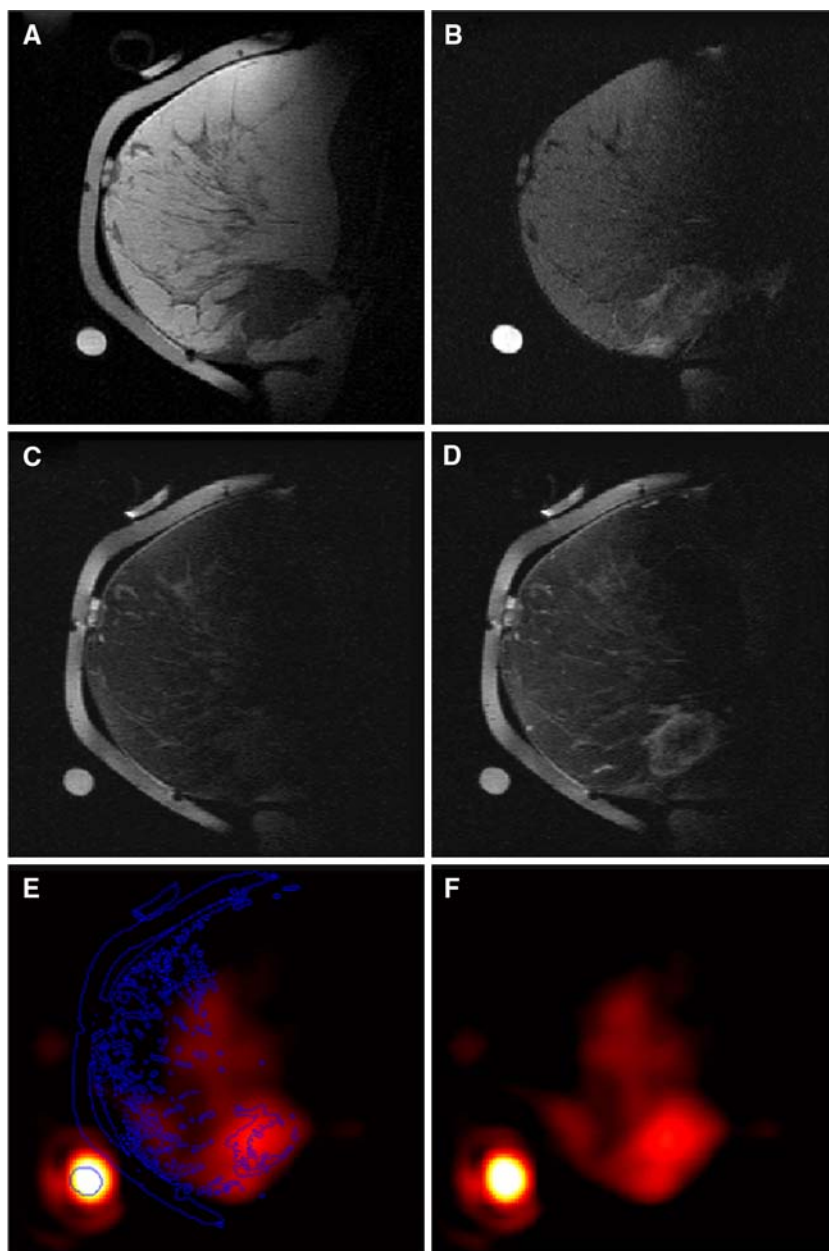


Fig. 3 ^1H and ^{23}Na images from a 54-year-old patient (#11) with 5.5 cm infiltrating poorly differentiated ductal carcinoma (T3) at the 12 o'clock position in the left breast. (A) Fat-suppressed T2W ^1H image shows mass with T_2 intermediate signal and edematous T_2 bright retroareolar glandular tissue (arrow); (B) co-registered,

fat-suppressed, T1W image post-Gd injections with level contours in yellow shows enhancement of the mass at 12 o'clock and no enhancement in the retroareolar glandular tissue; (C) co-registered ^{23}Na image with level contours from (B) superimposed in blue. Region with edema is indicated by a green arrow

Fig. 4 A complete set of registered sagittal ^1H - and ^{23}Na images from a 63-year-old patient (#16) with infiltrating, poorly differentiated, ductal carcinoma with necrosis (**A**) T1W, (**B**) T2W fat-suppressed, (**C**) pre-contrast FSPGR T1W. (**D**) Post-contrast FSPGR T1W. (**E** and **F**) ^{23}Na MRI with (**E**) and (**F**) without level contours (blue lines) copied from the post-contrast image



with a spatial resolution of 0.2 ml in under 13 min. Whether the approximately 50% increase in TSC in malignant lesions is due to changes in intracellular sodium content and/or to changes in EVF cannot be concluded from this study, but the magnitude of the changes indicate that the sodium level detected by this technique is highly specific for malignancy.

The fraction of the TSC that corresponds to intracellular sodium depends on both the IVF and the sodium concentrations in each compartment. Normal $[\text{Na}]_{\text{ex}}$ is not known for glandular tissue, but between cell types and even species, all values appear to be in the range of 8–15 mmol/l. For the purpose of this

discussion we estimate a value of 12 mmol/l based on values of 12 mmol/l reported for hepatocytes [31], erythrocytes [13, 32], and 10–12 mmol/l in mouse astrocytes [33]. Assuming a 140 mmol/l extracellular sodium concentration, $[\text{Na}]_{\text{ex}}$ [34] and the estimated 12 mmol/l intracellular sodium concentration, $[\text{Na}]_{\text{in}}$ for normal glandular tissue, the measured TSC in glandular tissue (Table 1) would be consistent with an 18% EVF and a 28% intracellular sodium contribution to TSC². Microscopy studies of lobular structures of

² Assuming $\text{TSC} = (1-\text{EVF}) \cdot [\text{Na}]_{\text{in}} + \text{EVF} \cdot [\text{Na}]_{\text{ex}}$ with $\text{EVF} = 1 - \text{IVF}$.

Table 1 TSC found in patients with benign and malignant lesions expressed in mmol/l tissue and as TSC ratios

Patient # Biopsy findings	Age		TSC mmol/l			TSC ratios		
	Cat.	Years	Lesion	Gland	Adipose	Lesion/gland	Lesion/adipose	Gland/adipose
1 Fibroadenoma, benign lesion	0	42	31.7	23.2	16.5	1.4	1.9	1.4
2 Fibroadenoma, benign lesion	0	41	24.1	34.0	6.0	0.7	4.0	5.7
3 Proliferative fibrocystic change and sclerosing adenosis	0	55	21.6	37.3	8.9	0.6	2.4	4.2
4 Infiltrating ductal carcinoma	1	43	79.4	49.6	13.6	1.6	5.9	3.7
5 Invasive ductal carcinoma	1	49	54.7	46.8	20.6	1.2	2.7	2.3
6 Infiltrating poorly differentiated ductal carcinoma	1	51	34.8	29.8	14.6	1.2	2.4	2.0
7 Invasive ductal carcinoma	1	38	74.0	74.0	74.0	1.0	1.0	1.0
8 Infiltrating ductal carcinoma	1	35	37.8	15.4	10.1	2.5	3.7	1.5
9 Invasive ductal carcinoma	1	54	42.4	–	7.1	–	5.9	–
10 Infiltrating poorly differentiated ductal carcinoma + necrosis	1	63	79.3	–	9.5	–	8.4	–
11 Infiltrating ductal carcinoma	1	68	61.8	42.3	20.4	1.5	3.0	2.1
12 Poorly differentiated infiltrating mammary carcinoma	1	54	38.1	16.1	9.6	2.4	3.9	1.7
13 Infiltrating moderately differentiated adenocarcinoma	1	61	62.4	35.4	14.7	1.8	4.2	2.4
14 In situ and infiltrating ductal carcinoma	1	54	42.6	33.6	15.9	1.3	2.7	2.1
15 In situ and infiltrating ductal carcinoma	1	41	30.0	21.0	16.4	1.4	1.8	1.3
16 In situ and infiltrating ductal carcinoma	1	72	74.7	29.9	10.8	2.5	6.9	2.8
17 In situ and infiltrating ductal carcinoma	1	39	55.6	28.2	16.4	2.0	3.4	1.7
18 Infiltrating lobular carcinoma	2	59	66.8	42.4	8.1	1.6	8.2	5.2
19 Infiltrating lobular carcinoma	2	41	58.5	36.6	10.3	1.6	5.7	3.6
20 Infiltrating lobular carcinoma	2	58	33.3	27.9	12.9	1.2	2.6	2.2
21 Infiltrating lobular carcinoma	2	48	42.5	–	20.0	–	2.1	–
22 DCIS with calcifications	3	66	40.8	27.0	17.1	1.5	2.4	1.6
Mean	51	53	26	34	16	1.63	4.05	2.54
St. dev.	11	16	5	13	14	0.47	2.17	1.35
Min.	35	30.0	21.6	15.4	6.0	1.0	1.0	1.0
Max.	72	79.4	31.7	74.0	74.0	2.5	8.4	5.7
N	22	19	3	19	22	16	19	18
		a	b	c	a	a	c	a

TSC and standard deviations of the means for all patients are given for adipose and uninvolved glandular tissue (except in patients #16, 17, and 21, where no TSC reading for uninvolved glandular tissue could be determined). The mean TSC in lesions (in bold) is calculated separately for malignant ($N = 19$) and benign lesions ($N = 3$)

^a All subjects, category 0–3

^b Benign lesions, category 0 only

^c Malignant lesions, category 1–3 only

normal human breast tissue report that the volume fraction of the ductal lumen is less than 4%, and that of the blood vessels is about 2%, independent of age (20–60 years old; $N = 58$) [35]. This would imply an EVF contribution from the vessels and lumens of only 6%, with the remaining 12% made up by interstitial volume in normal tissue.

Because $[\text{Na}]_{\text{ex}}$ cannot change, the observed 63% increase in TSC in malignant tissue would correspond to either an increase in $[\text{Na}]_{\text{in}}$ of 3.2-fold to 38 mmol/l, assuming EVF is constant; or to an almost doubling of the EVF to 34% if $[\text{Na}]_{\text{in}}$ is assumed constant; or some combination of both. The EVF in malignant tumors could be expected to increase with vascularization and

increased interstitial space. Unfortunately, there is no acceptable, noninvasive way to directly determine EVF in human breast tissue, but estimates for lesions are available from dynamic CE MRI studies [36]. Using a model parameter fit, the mean interstitial volume fraction for malignant tumors was estimated as ~ 0.34 , with a plasma volume fraction of about 0.2 [36]. This might imply a total EVF of 0.54, which is very high and would not match the microscopic appearance of breast lesions [37, 38], let alone our maximum EVF estimate of 31% by ^{23}Na MRI. Either way, by both dynamic CE and ^{23}Na MRI considerations, it is likely that most of the increased TSC observed in malignant lesions is at least, in large part, due to increases in EVF.

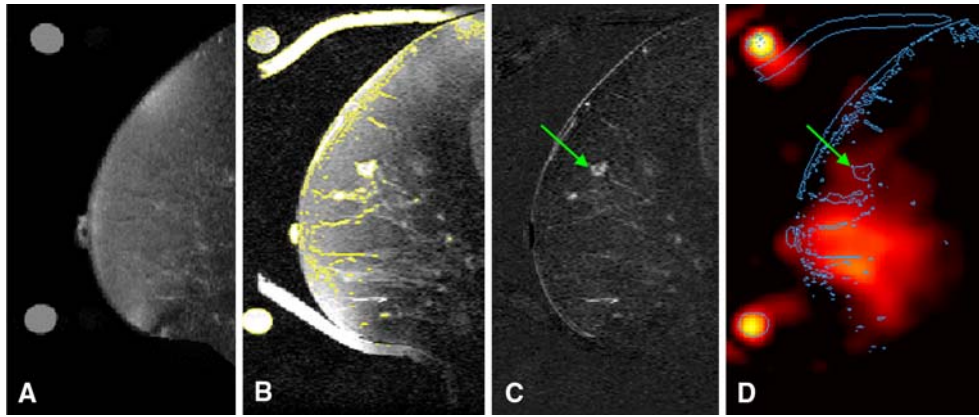


Fig. 5 ^1H and ^{23}Na images of a benign lesion (#3, proliferative fibrocystic change and sclerosing adenosis). (**A**) T2W fat-suppressed ^1H image; (**B**) fat-suppressed T1W image post-Gd injections with level contours in yellow; (**C**) difference image from fat-suppressed T1W images pre-Gd injection and post-Gd image (**B**); (**D**) registered ^{23}Na image with level contours from

(**B**) superimposed in blue. Green arrows indicate the position of the benign lesion which shows up clearly on the Gd-enhanced images (**B** and **C**), but not on the T2W or ^{23}Na images (**A** and **D**). The color scale of the ^{23}Na image was adjusted to obtain the level of the reference phantom signals approximately equal to those in Fig. 3C

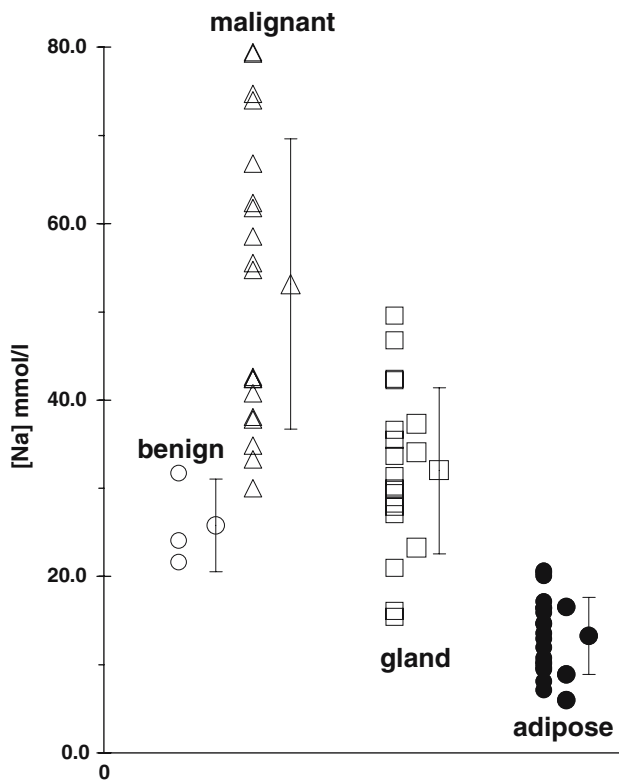


Fig. 6 TSC found in lesions and unaffected breast tissues in patients, and the corresponding means from all patients with error bars at $\pm\text{SD}$. Benign lesions: open circles. Malignant lesions: open triangles. Glandular tissue: open squares, and adipose tissue: closed circles. Data points for glandular tissue and adipose tissue in patients with benign lesions are slightly offset to the right, but were included in the means

On the other hand, the normal intracellular concentration is unlikely to be lowered in any diseased state, and elevations in $[\text{Na}]_{\text{in}}$, would presumably reduce the ATP needed to maintain the intra/extra-cellular sodium gradient in proliferating cells. ^{23}Na MRI of TSC in malignant lesions could provide a useful and independent adjunct to CE 1H MRI because it is directly sensitive to changes in EVF, and is not influenced by contrast agent delivery kinetics, the kinetic modeling, or the membrane permeability. In addition, TSC measurements are proportional to changes in $[\text{Na}]_{\text{in}}$ that are sensitive to cellular ion pump function, membrane integrity, and disease state. A reliable, independent means of measuring IVF or EVF would help determine the origin of the changes in TSC associated with malignancy.

While our data show some overlap between the TSC of malignant tumors, and the TSC in unaffected glandular tissue (Fig. 6), the ratio of TSC in malignant lesions to that in unaffected glandular or adipose tissue is consistently higher than unity, as indexed by the highly significant paired statistical differences (Table 1). This observation offers hope that the technique may help differentiate malignant tumors from benign lesions when used in conjunction with other imaging parameters [39]. The scatter in TSC in normal tissues greatly exceeds that attributable to SNR alone, and is therefore likely attributable to heterogeneity among subjects, as well as to tissue heterogeneity within the 6 mm (isotropic) ^{23}Na MRI voxels in breasts with few areas comprised of solely glandular or of adipose tissue.

We conclude that TSC, as measured and imaged by quantitative noninvasive ^{23}Na MRI at 1.5 Tesla, is significantly higher in malignant lesions than in normal glandular and adipose tissues, and apparently, benign lesions as well. We are presently expanding our studies to a larger patient population to determine whether TSC images can significantly improve the specificity of lesion detection in the context of an integrated CE MRI breast protocol, and to investigate the correlation between sodium levels and tumor changes in response to therapy.

Authors' contributions

RO and MAJ: Study conception and design, data collection and data analysis, manuscript writing, and financial support; MAJ: Study design, data collection and data analysis, and financial support; ACW, VS, SDM, NFK: Provision of study material or patients and collection and assembly of data. KJM, DAB, data processing and MRI reading; PAB: study design manuscript revision, and financial support.

Acknowledgments This work was supported by NIH grants R21CA095907, 1R01CA100184, P50CA103175 ACS Grant IRS-58-005-40. The authors would like to thank Cynthia Schultz and Cynthia Maranto and Donna Hardy for their vital support in interactions with patients and in running MR protocols.

References

- Schnall MD, Blume J, Bluemke DA, DeAngelis GA, DeBruhl N, Harms S et al (2006) Diagnostic architectural and dynamic features at breast MR imaging: multicenter study. *Radiology* 238(1):42–53
- Bluemke DA, Gatsonis CA, Chen MH, DeAngelis GA, DeBruhl N, Harms S et al (2004) Magnetic resonance imaging of the breast prior to biopsy. *JAMA* 292(22):2735–2742
- Lee CH (2004) Problem solving MR imaging of the breast. *Radiol Clin North Am* 42(5):919–934, vii
- Kuhl CK (2000) MRI of breast tumors. *Eur Radiol* 10(1):46–58
- Rankin SC (2000) MRI of the breast. *Br J Radiol* 73(872):806–818
- Jacobs MA, Barker PB, Bottomley PA, Bhujwalla Z, Bluemke DA (2004) Proton magnetic resonance spectroscopic imaging of human breast cancer: a preliminary study. *J Magn Reson Imaging* 19(1):68–75
- Jacobs MA, Barker PB, Argani P, Ouwerkerk R, Bhujwalla ZM, Bluemke DA (2005) Combined dynamic contrast enhanced breast MR and proton spectroscopic imaging: a feasibility study. *J Magn Reson Imaging* 21(1):23–28
- Stanwell P, Gluch L, Clark D, Tomanek B, Baker L, Giuffre B et al (2005) Specificity of choline metabolites for in vivo diagnosis of breast cancer using ^1H MRS at 1.5 T. *Eur Radiol* 15(5):1037–1043
- Katz-Brull R, Lavin PT, Lenkinski RE (2002) Clinical utility of proton magnetic resonance spectroscopy in characterizing breast lesions. *J Natl Cancer Inst* 94(16):1197–1203
- Kim RJ, Lima JAC, Chen EL, Reeder SB, Klock FJ, Zerhouni EA et al (1997) Fast Na-23 magnetic resonance imaging of acute reperfused myocardial infarction—Potential to assess myocardial viability. *Circulation* 95(7):1877–1885
- Ouwerkerk R, Bleich KB, Gillen JS, Pomper MG, Bottomley PA (2003) Tissue sodium concentration in human brain tumors as measured with ^{23}Na MR Imaging. *Radiology* 227:529–537
- Nissen H, Jacobsen JP, Horder M (1990) A review of ^{23}Na nuclear magnetic resonance spectroscopy for the in vitro study of cellular sodium metabolism. *Scand J Clin Lab Invest* 50(5):497–507
- Ouwerkerk R, Vanechteld CJA, Staal GEJ, Rijksen G (1989) Erythrocyte Na^+/K^+ ATPase activity measured with Na-23 NMR. *Magn Res Med* 12(2):164–171
- Fraser SP, Diss JK, Chioni AM, Mycielska ME, Pan H, Yamaci RF et al (2005) Voltage-gated sodium channel expression and potentiation of human breast cancer metastasis. *Clin Cancer Res* 11(15):5381–5389
- Leach MO (2001) Application of magnetic resonance imaging to angiogenesis in breast cancer. *Breast Cancer Res* 3(1):22–7
- Reshkin SJ, Bellizzi A, Albarani V, Guerra L, Tommasino M, Paradiso A et al (2000) Phosphoinositide 3-kinase is involved in the tumor-specific activation of human breast cancer cell Na^+/H^+ exchange, motility, and invasion induced by serum deprivation. *J Biol Chem* 275(8):5361–5369
- Bhujwalla ZM, Artemov D, Natarajan K, Ackerstaff E, Solaiyappan M (2001) Vascular differences detected by MRI for metastatic versus nonmetastatic breast and prostate cancer xenografts. *Neoplasia* 3(2):143–153
- Lagarde AE, Pouyssegur JM (1986) The $\text{Na}^+:\text{H}^+$ antiport in cancer. *Cancer Biochem Biophys* 9(1):1–14
- Cameron IL, Smith NKR, Pool TB, Sparks RL (1980) Intracellular concentration of sodium and other elements as related to mitogenesis and oncogenesis in vivo. *Cancer Res* 40(5):1493–1500
- Ignelzi RJ (1983) An analysis of the nuclear sodium content of human normal glia as well as tumors of glial and nonglial origin. *Neurol Res* 5(2):79–84
- Pieri C, Giuli C, Bertoni-Freddari C (1983) X-ray microanalysis of monovalent electrolyte contents of quiescent, proliferating as well as tumor rat hepatocytes. *Carcinogenesis* 4(12):1577–1581
- Reshkin SJ, Bellizzi A, Caldeira S, Albarani V, Malanchi I, Poignee M et al (2000) Na^+/H^+ exchanger-dependent intracellular alkalinization is an early event in malignant transformation and plays an essential role in the development of subsequent transformation-associated phenotypes. *Faseb J* 14(14):2185–2197
- Kometiani P, Liu L, Askari A (2005) Digitalis-induced signaling by Na^+/K^+ -ATPase in human breast cancer cells. *Mol Pharmacol* 67(3):929–936
- Ng KH, Bradley DA, Looi LM (1997) Elevated trace element concentrations in malignant breast tissues. *Br J Radiol* 70(832):375–382
- Ouwerkerk R, Jacobs MA, Bottomley PA, Fajardo LL (2002) A method for quantifying tissue sodium in breast tumors with short echo time ^{23}Na MRI and co-registered proton images. In: Proceedings of the tenth meeting of the international society of magnetic resonance in medicine, Honolulu, HI, p 2061

26. Jacobs MA, Ouwerkerk R, Wolff AC, Stearns V, Bottomley PA, Bluemke DA et al (2004) Monitoring primary systemic therapy in locally advanced breast cancer using proton and sodium magnetic resonance imaging. In: Proceedings of the twelfth meeting of the international society of magnetic resonance in medicine, Kyoto, Japan, p 246
27. Boada FE, Gillen JS, Shen GX, Chang SY, Thulborn KR (1997) Fast three dimensional sodium imaging. *Magn Reson Med* 37(5):706–715
28. Ouwerkerk R, Weiss RG, Bottomley PA (2005) Measuring human cardiac tissue sodium concentrations using surface coils, adiabatic excitation, and twisted projection imaging with minimal T2 losses. *J Magn Reson Imaging* 21(5):546–555
29. Schomberg H, Timmer J (1995) The gridding method for image-reconstruction by Fourier transformation. *IEEE Trans Med Imaging* 14(3):596–607
30. Perneger TV (1998) What's wrong with Bonferroni adjustments. *BMJ* 316(7139):1236–1238
31. Lidofsky SD, Xie MH, Sostman A, Scharschmidt BF, Fitz JG (1993) Vasopressin increases cytosolic sodium concentration in hepatocytes and activates calcium influx through cation-selective channels. *J Biol Chem* 268(20):14632–14636
32. Deluise M, Flier JS (1986) Functionally abnormal Na⁺-K⁺ pump in erythrocytes of a morbidly obese patient. *J Clin Invest* 69(1):38–44
33. Chatton JY, Shimamoto K, Magistretti PJ (2001) Effects of glial glutamate transporter inhibitors on intracellular Na⁺ in mouse astrocytes. *Brain Res* 893(1–2):46–52
34. Olson BR, Forman MR, Lanza E, McAdam PA, Beecher G, Kimzey LM et al (1996) Relation between sodium balance and menstrual cycle symptoms in normal women. *Ann Intern Med* 125(7):564–567
35. Hutson SW, Cowen PN, Bird CC (1985) Morphometric studies of age related changes in normal human breast and their significance for evolution of mammary cancer. *J Clin Pathol* 38(3):281–287
36. Brix G, Kiessling F, Lucht R, Darai S, Wasser K, Delorme S et al (2004) Microcirculation and microvasculature in breast tumors: pharmacokinetic analysis of dynamic MR image series. *Magn Reson Med* 52(2):420–429
37. Wellings SR, Jensen HM, Marcum RG (1975) An atlas of subgross pathology of the human breast with special reference to possible precancerous lesions. *J Natl Cancer Inst* 55(2):231–273
38. Squartini F, Bistocchi M, Buongiorno L (1981) Development, morphology, and progression of mammary tumors during and after fertile life in BALB/cfRIII mice. *J Natl Cancer Inst* 66(2):311–319
39. Jacobs MA, Ouwerkerk R, Wolff AC, Stearns V, Bottomley PA, Barker PB et al (2004) Multiparametric and multinuclear magnetic resonance imaging of human breast cancer: current applications. *Technol Cancer Res Treat* 3(6):543–550